Graphical Abstract

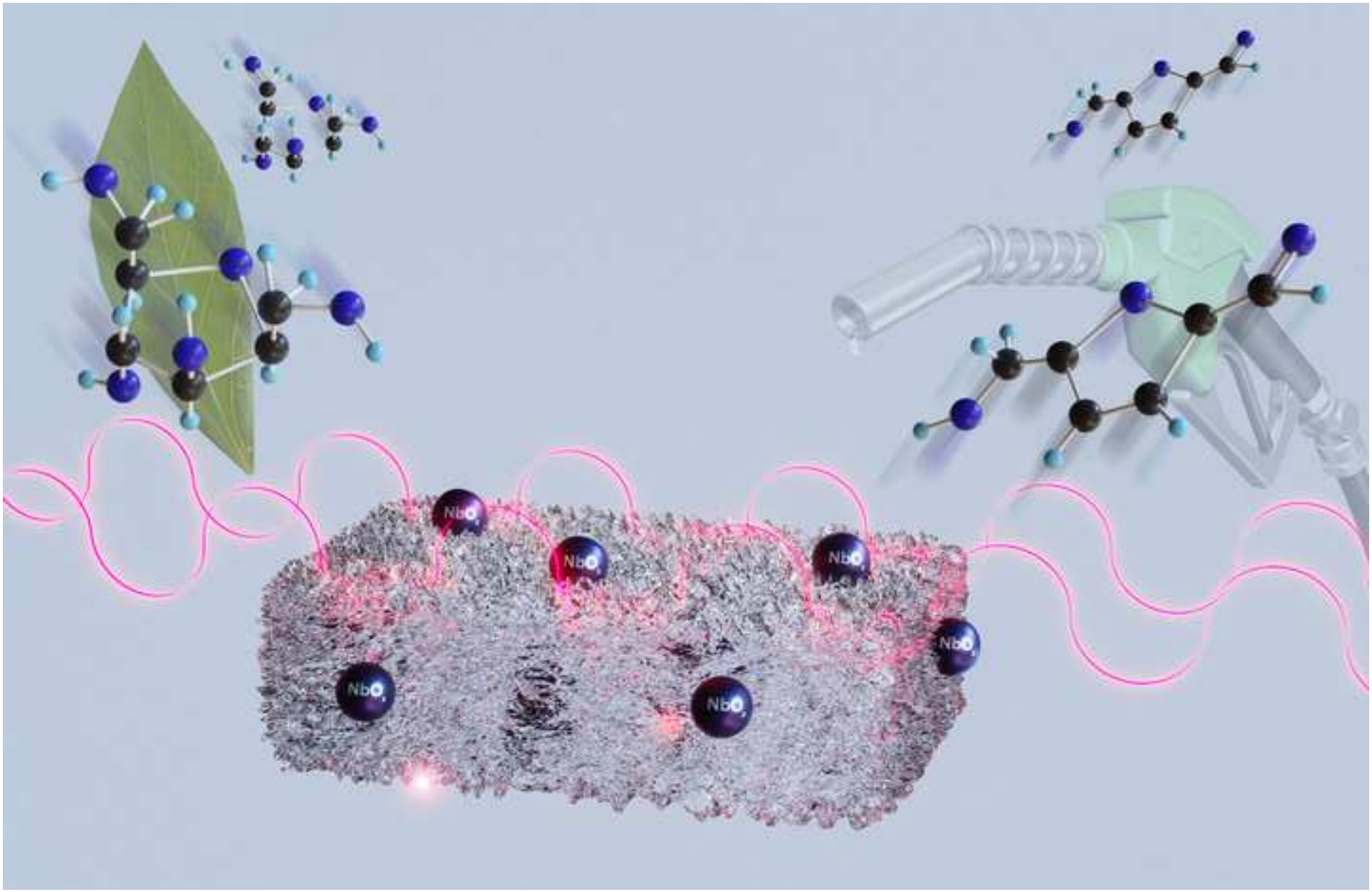

Highly porous niobium-containing glasses as catalysts for microwave-assisted rapid conversion of sugars into HMF

Highlights

- Highly porous silica glasses allow for high surface dispersion of niobium oxide.
- Niobium-containing mesoporous glass catalyzes the dehydration of fructose to HMF.
- Fast and efficient conversion of fructose is obtained by microwave irradiation.
- Low loading of Nb on the glass matrix allows tailoring Lewis and Brønsted acid sites.

Highly porous niobium-containing glasses as catalysts for microwave-assisted rapid conversion of sugars into HMF

Maria J. F. Costa,[a,c,e,f] Alexandre A. S. Gonçalves,[b] Roberto Rinaldi,[c] Henrik Bradtmüller,[d] Hellmut Eckert,*[e,f] and Eduardo B. Ferreira,*[a,f]

Affiliations:

[a] Department of Materials Engineering, São Carlos School of Engineering, University of São Paulo, São Carlos, 13566-590 São Paulo, Brazil

[b] Catalytic and Process Ceramics, Saint-Gobain NorPro, Stow, 44224 Ohio, USA

[c] Department of Chemical Engineering, Imperial College London, South Kensington Campus, SW7 2AZ London, UK

[d] Department of Materials, Federal University of Sao Carlos, São Carlos, 13566-905 São Paulo, Brazil

[e] São Carlos Institute of Physics, University of São Paulo, São Carlos, 13566-590 São Paulo, Brazil

[f] Center for Research, Technology and Education in Vitreous Materials, CeRTEV/FAPESP

*E-mail: mariacosta.ufrn@gmail.com, ebferreira@sc.usp.br and eckert@ifsc.usp.br

Graphic abstract

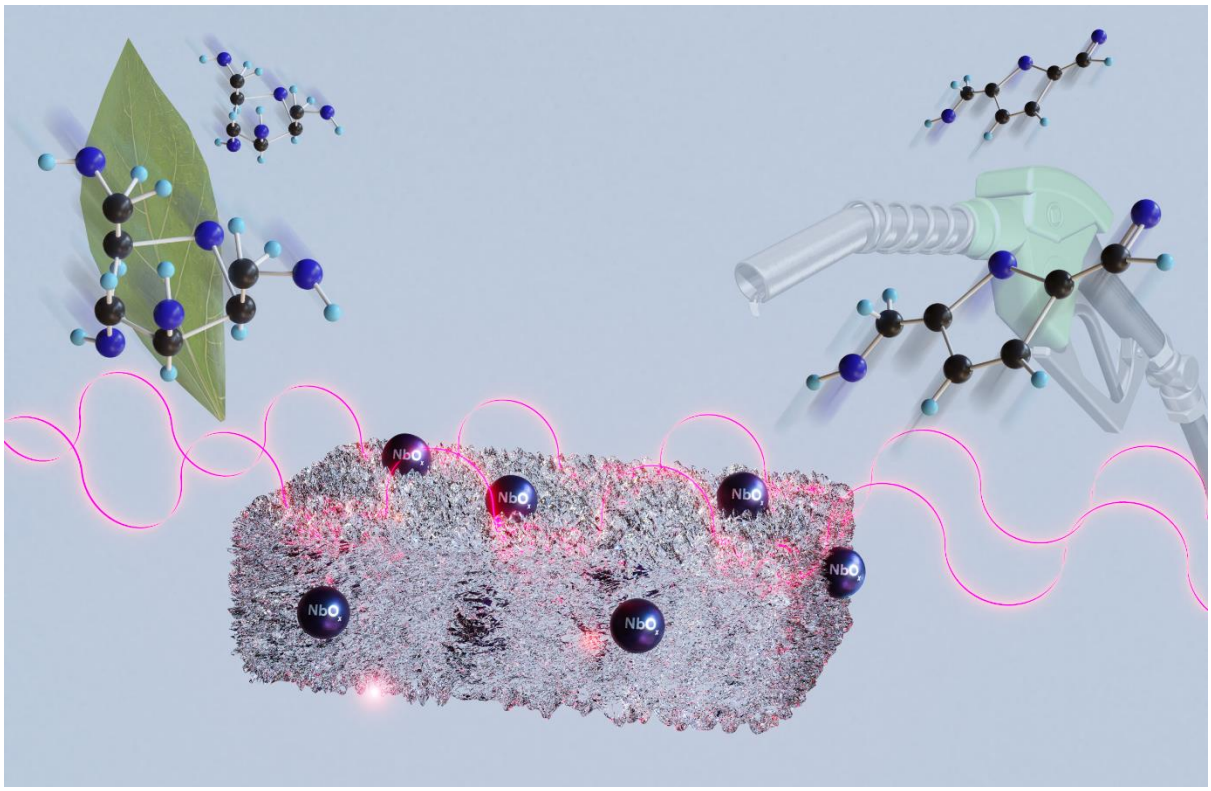

Highlights

- Highly porous silica glasses allow for high surface dispersion of niobium oxide.
- Niobium-containing mesoporous glass catalyzes the dehydration of fructose to HMF.
- Fast and efficient conversion of fructose is obtained by microwave irradiation.
- Low loading of Nb on the glass matrix allows tailoring Lewis and Brønsted acid sites.

Abstract: The conversion of sugars into furfurals represents a crucial step towards sustainability in the production of biobased fuels and chemicals. Herein, a series of porous silica-based glasses decorated with niobium oxide was prepared, thoroughly characterized, and employed in the microwave-assisted catalytic conversion of hexoses into 5-hydroxymethylfurfural (HMF) at low temperatures. The glasses were designed by sol-gel synthesis utilizing an ionic liquid, 1-butyl-3-methylimidazolium tetrafluoroborate, as a catalytic agent for phase condensation. Decoration with niobium(V) surface oxide performed by wet impregnation at considerably low concentrations followed by thermal treatment is shown to improve metal dispersion toward near single-atom catalysts, consequently changing surface chemistry by creating Lewis and Brønsted acid sites for the selective conversion of fructose into HMF. Lowering niobium loading decreases the amount of Lewis acid sites, resulting in increased HMF selectivity, thus mitigating humin formation. Moreover, the high niobium dispersion delivered superior HMF productivity than those of reference materials.

Keywords: HMF • porous glass • niobium oxide • dehydration of fructose • humin

1. Introduction

The efficient and economically viable production of fuels and chemicals from vastly abundant lignocellulosic wastes (e.g., sugarcane bagasse, corn stover) is one of the most significant challenges for sustainability due to the complexity of biomass substrate materials [1–4]. In this context, converting glucose and fructose into 5-hydroxymethylfurfural (HMF) is crucial for producing key furan derivatives (*e.g.*, 2,5-furan-dicarboxylic acid or 2,5-dimethylfuran) [5–7]. Acid catalysis plays an essential role in synthesizing HMF from hexoses and cellulose. Indeed, both the hydrolysis of lignocellulosic materials and the subsequent conversion of the produced mono- and oligo-hexoses to furan derivatives are promoted by solid acid catalysts. Examples include polyoxometalates, sulfonated silica, zeolites [8–12], sulfated zirconia [13], hybrid organic-inorganic anatase [14], and most recently, mesoporous vanadium and niobium oxides [15,16] and their oxyphosphates $VOPO_4 \cdot xH_2O$, $NbOPO_4 \cdot xH_2O$ [9,17]. These materials are distinguished by their high stability towards the aqueous medium and their activity in converting fructose into 5-hydroxymethylfurfural (HMF), making them exciting candidates for directly converting lignocellulosic material into HMF by one-pot reactions [9].

Several niobium oxide-containing materials have been reported to catalyze the conversion of glucose and fructose into HMF [9,18–26]. A key feature of those materials is the presence of water-tolerant Lewis acid sites [9,16]. However, several challenges persist and must be addressed to create commercially viable catalysts, namely: (I) the degree of porosity in pure oxides or phosphates is limited; (II) the limited porosity poses mass-transfer limitations in fast reactions as those assisted by microwave heating; and (III) the high density of acid sites may favor the formation of humins (undesired byproducts).

Some degree of porosity is expected for any material containing high concentrations of heavy metal oxides due to the several oxidation states for such metals. This is the case of NbO_x phases, which comprise several thermodynamically stable oxides and various mixed-valence compounds (e.g., NbO, NbO_2, Nb_2O_5) [27]. Phase transitions and changes in the Nb oxidation state promote mass transfer, enhancing sintering with densification [28], which lowers porosity. The limitation of porosity in bulk heavy metal oxides (e.g., Nb_2O_5) is often overcome by supporting the metal oxide phase in highly porous supports (e.g., mesoporous silica or alumina materials) [21,29,30]. Silica-based supports, especially in the glassy state, are considerably less acidic than other oxides and, therefore, may present higher stability under conditions of carbohydrate conversion [31]. Moreover, the metal oxide dispersion can be tuned from single-atom sites to thin layers a few nanometers thick, depending on metal loading and interactions between the pore surface of the support and the metal oxide [32,33]. As substantial changes in the active catalytic sites occur upon increasing metal dispersion [33], one requires extensive characterization of the materials to understand the mechanisms underlying the effect of metal dispersion on a catalytic conversion [9,16].

A well-balanced distribution of Lewis and Brønsted acid sites for converting hexoses into HMF was consistently demonstrated to be a unique feature of Nb-based catalysts, mitigating side reactions forming humins [34]. Zhang *et al.* [9] demonstrated that Lewis acid sites are essential to isomerizing glucose into fructose and Brønsted acid sites are detrimental to this process. However, Brønsted acid sites are required to dehydrate fructose to HMF. Despite this, high concentrations of Brønsted acid sites favor the formation of humins. Notably, Lewis acid sites can be transformed into Brønsted acid sites upon water sorption and partial hydrolysis,

depending on the water stability of the catalytic phase. When this process extensively takes place, the conversion of glucose to fructose is dramatically affected.

This work reports the synthesis and characterization of materials with a high degree of porosity and tailored nature and density of acid sites to catalyze the selective conversion of hexoses into HMF. The synthesis of porous glasses with the internal pore-surface decorated with niobium oxide began with silica precursors obtained via sol-gel synthesis. By wet impregnation followed by thermal treatment, niobium oxide species were grafted on the silica support. The materials structure and surface features were characterized by low-temperature N_2 sorption, pyridine sorption followed by attenuated total reflectance-Fourier transform infrared spectroscopy (ATR-FT-IR), inductively coupled plasma optical emission spectrometry (ICP-OES), and thermogravimetry (TG). In addition, the local structure of the niobium oxide phase was studied using solid-state nuclear magnetic resonance spectroscopy (SS-NMR). The materials were applied to convert hexoses into HMF. The reactions were carried out in a biphasic system heated by microwave radiation. The catalytic activity correlated with the nature of acid sites and Nb loading. In the broader context, this work addresses issues not yet well described in the current literature, correlating the acidity nature and concentration of niobium oxide with fructose conversion, HMF selectivity and productivity, and humins formation.

2. Experimental Section

2.1. Catalyst preparation

Materials. Niobium(V) chloride 99% (Sigma-Aldrich), triblock copolymer Pluronic® P123 $(EO)_{20}(PO)_{70}(EO)_{20}$ (BASF), TEOS ≥99% (Sigma-Aldrich), diammonium hydrogen phosphate A.R. (Neon), phosphoric acid 85% (Synth), and niobium(V) ethoxide 99.95% (Sigma-Aldrich) were used as starting materials.

Preparation of the mesoporous silica glass support. The synthesis of mesoporous silica glass adapted the procedure reported by Queiroz et al. [35]. Typically, TEOS (9.8 g, ≥99% Sigma-Aldrich), ethanol (2.4 mL, 99.8% Neon), and distilled water (2.4 mL) were combined with a 0.1 M HCl aqueous solution (0.88 mL). The mixture was stirred at room temperature for 2 h. Afterwards, 1-butyl-3-methylimidazolium tetrafluoroborate (4.2 mL, ≥97.0% Sigma-Aldrich) was added. After an additional 10 min of stirring, the solution was poured into a Petri dish. A gel phase was formed after 1 day. The gel was kept under ambient conditions for 1 week and then annealed at 50 °C for 2 days and at 120 °C for an additional 2 days. The ionic liquid was extracted via Soxhlet extraction in acetonitrile for 2 days, and the sample was heated again at 120 °C for another additional 2 days.

Grafting of Nb(V) oxide on the mesoporous glass surface. Nb(V) oxide was grafted on mesoporous glass by wet impregnation [36] (**Scheme S1**, Supporting Information), employing a methanol solution of niobium(V) chloride (10 mL, $NbCl_5$, 99% Sigma-Aldrich) at a concentration of 7.7 mM (for the synthesis of 1.8%Nb-MG) and 12 mM (for the synthesis of 2.8%Nb-MG). The impregnation was performed at 60 °C for 12 h, followed by rotoevaporation until complete dryness. The final solids were dried at 100 °C overnight, then calcined under an air atmosphere at 500 °C for 6 h. Nominal niobium contents in wt% are denoted "*x*" using sample labels *x*%Nb-MG.

2.2. Reference Materials

Mesoporous niobium silicate Nb-SBA-15 (Si/Nb=15) was synthesized by the hydrothermal method, based on an experimental procedure described by Trejda *et al*. [37], using the molar composition of 1TEOS:0.070Nb:0.017P123:170.5H_2O. First, niobium(V) chloride (0.39 g) was dissolved in water (63 mL), followed by the addition of P123 (2.0 g). After the complete dissolution of the polymer, TEOS (4.55 mL) was added, and the mixture was stirred at 40 °C overnight. Next, the resulting mixture was transferred to a Teflon-lined stainless steel autoclave and kept at 100 °C for 24 h. After that, the solid was filtered, washed with deionized water, and dried at room temperature. Finally, the obtained solid was subjected to calcination under an air atmosphere at 550 °C for 6 h, using a heating rate of 3 °C·min^{-1} in N_2 atmosphere.

Mesoporous niobium oxyphosphate ($NbOPO_4$) was also obtained by a hydrothermal method following the procedure reported elsewhere [38]. First, diammonium hydrogen phosphate (1.32 g) was dissolved in water (20 mL). Next, phosphoric acid (4.7 mL) was added to the solution to adjust the pH to 2. Then, under vigorous stirring, the solution was added to 40 mL of 0.2 M niobium ethoxide (2 mL) aqueous solution. An aqueous solution of P123 (containing 0.43 g of P123 dissolved in 13 mL of a 2 M HCl solution) was then slowly added to this solution. The resulting mixture was stirred at 35 °C for 1 h, transferred to a Teflon-lined stainless steel autoclave, and kept at 160 °C for 24 h. After cooling, the solid was filtered, washed with deionized water, and dried at room temperature. The final solid was heated to 550 °C in N_2 atmosphere at a heating rate of 3 °C·min^{-1} and subsequently calcined in air at 550 °C for 6 h.

2.3. Materials characterization

Low-temperature nitrogen physisorption. Measurements were performed using a Micromeritics ASAP 2020 volumetric adsorption analyzer at -196 °C. The samples were outgassed at 200 °C for 2 h under reduced pressure before each measurement. The specific surface area (S_{BET}), the total pore volume (V_t), and the pore size distribution (PSD) was calculated using the adsorption branches of isotherms. The specific surface areas were calculated according to the Brunauer–Emmett–Teller (BET) method using adsorption data in the relative pressure P/P_0 range of 0.05–0.2. The total pore volumes (V_t) were estimated from the amount adsorbed at the relative pressure of 0.98. Finally, the pore size distributions (w_{KJS}) were calculated from nitrogen adsorption isotherms' adsorption branches using the improved KJS method [39].

Determination of the acid site nature. The procedure used for acidity measurement by ATR-FT-IR was previously reported [40]. Typically, pyridine adsorption experiments were performed in a reactor containing 50 mg of material, which was activated initially at 300 °C, under N_2 flowing at a rate of 100 $mL \cdot min^{-1}$ for 1 h. After this activation, the temperature was decreased to 150 °C, and the N_2 flow was directed to a saturator containing liquid pyridine. Next, the pyridine-saturated N_2 stream was redirected to the reactor containing the sample for 1 h. Afterward, an N_2 flow was passed over the samples for 1 h to remove physically adsorbed pyridine. Then, ATR-FT-IR spectra were collected on a Bruker Tensor 27 FT-IR spectrometer using a Pike Miracle single bounce attenuated total reflectance (ATR) cell equipped with a ZnSe single crystal detector.

Determination of the acid site distribution by acid strength. The procedure used to determine the total acidity by TG is reported elsewhere [41–44]. The pyridine adsorption method is stated above. Typically, TG analysis is performed to determine

the distribution of acid sites according to the acid strength. We used a TGA/DSC (Mettler-Toledo) with N_2 as a gas carrier flowing at 25 mL·min^{-1}. The samples were heated from room temperature up to 800 °C, at a heating rate of 10 °C·min^{-1}. The acid sites' strength was distinguished as weak, medium, or strong by the pyridine mass-loss at 30-100 °C, 100-300 °C, and 300-550 °C, respectively.

Structural characterization by solid-state NMR. ^{29}Si magic-angle spinning (MAS) NMR experiments were recorded at a Larmor frequency of 48.1 MHz (magnetic flux density of 5.7 T) using an Agilent DD2 spectrometer. Spectra were measured in a 7.5 mm probe operated at a spinning frequency of 5.0 kHz, using 90° pulses of 8 µs duration, and 364 to 768 scans were collected at a recycle delay of 120 s. ^{29}Si chemical shifts are reported relative to tetramethylsilane (TMS). Solid kaolinite (-91.5 ppm) was employed as a secondary reference. Static ^{93}Nb NMR experiments were measured at a Larmor frequency of 97.9 MHz (magnetic flux density of 9.4 T) using a Bruker Avance III Neo spectrometer and Carr-Purcell-Meiboom Gill echo train acquisition [45] enhanced by wideband excitation [46]. The latter was accomplished using a train of identical WURST (wideband uniform rate smooth truncation) [47] pulses of 50 µs duration at a nutation frequency of 9.5 kHz and a shape factor of N = 80. The WCPMG spectra are shown after co-addition and Fourier transformation of the individual echoes. Chemical shifts were determined by having a saturated solution of $NbCl_5$ in acetonitrile (MeCN) as a reference.

Niobium content determination. Inductively coupled plasma optical emission spectrometry (ICP-OES) was employed for the elemental analysis of Nb-containing samples using an iCAP™ 7400 ICP-OES Analyzer - Thermo Fisher Scientific. The stock digestion solution was HNO_3:HF (3:2, v/v). The sample digestion was conducted in a microwave digester (CEM Corp., MarsXpress). The microwave

digestion settings were 200 °C, pressure: 800 psi, ramp time: 15 min, and hold time: 25 min.

2.4. Activity Tests

Microwave-assisted conversion of carbohydrates. The experiments were performed using a Monowave 300 microwave system (Anton Paar, Graz, Austria). The microwave-assisted experiments included pressure control and an automatic cooling process. The temperature was monitored with a fast responding ruby thermometer immersed into the reaction mixture and an IR temperature sensor measuring the glass reactor vial's surface temperature. The volume of the glass reaction vial was 10 mL. In a typical biphasic reaction experiment, the reaction vial was filled with catalyst (10 or 20 mg), methyl isobutyl ketone (3.5 mL, ≥98%, VWR Chemicals), and saturated sodium chloride solution containing fructose (≥99%, VWR Chemicals) or glucose (≥99%, Fisher Chemical at a concentration of 66 $mmol \cdot L^{-1}$ (1.5 mL) (**Figure S1**, Supporting Information). HMF is gradually produced in the aqueous phase and continuously extracted into the organic phase. The resulting mixture was subjected to microwave irradiation at 170 °C (ultra-fast heating) for 8 min under stirring at 300 rpm. As soon as the reaction time was completed, the glass reaction vial was cooled rapidly to room temperature to prevent further reactions. The resulting solution was filtered to retain any solid particle. After filtration, fructose and HMF concentrations were determined in both phases by high-performance liquid chromatography (HPLC).

HPLC analysis. HPLC experiments were carried out on a Shimadzu prominence liquid chromatography system (CBM-20A controller, SIL-20AC autosampler with cooling function, DGU-20A5 degassing unit, CTO-20AC column oven) equipped with

an evaporative light scattering detector (ELSD 3300, Alltech) to determine fructose and glucose concentrations, and a diode array UV-Vis detector (SPD-M30A detector, Shimadzu) to determine the HMF concentration. Samples from both phases from the biphasic reaction were collected. The aqueous phase containing fructose or glucose was analyzed using a *Prevail Carbohydrate ES* column (Grace Alltech, 250 mm × 4.6 mm, 5 µm) with an isocratic elution (mobile phase: acetonitrile/water, 70:30 v/v). The mobile phase flow rate was 1 mL·min^{-1}, the column oven temperature was kept at 30 °C, and the injection volume was 10 µL. In turn, both aqueous and organic phases from the reaction system were analyzed to determine the total concentration of HMF using a *Shim-pack XR-ODS column* (Shimadzu, 3 mm x 50 mm) with isocratic elution (mobile phase: acetonitrile/water, 20:80 v/v). The mobile phase flow was 0.5 mL min^{-1}, the column oven temperature was kept at 40 °C, and the injection volume was 1 µL. UV-Vis detection was carried out within the range of 190-800 nm. For quantification of HMF, the chromatogram traces measured at 275 nm were integrated. All HPLC analyses were duplicated **(Figures S2** and **S3**, Supporting Information). Calibration curves were obtained using reference standards. The following equations defined the conversion of the substrates, yield of products, and mass balance of the reaction:

$$Conversion_{\text{substrate}}\ (\%) = \frac{n_{\text{starting substrate}} - n_{\text{unreacted substrate}}}{n_{\text{starting substrate}}} \cdot 100\ \% \qquad (1)$$

$$Yield_{\text{HMF}}\ (\%) = \frac{n_{\text{HMF(aqueous phase)}} + n_{\text{HMF(organic phase)}}}{n_{\text{starting substrate}}} \cdot 100\% \qquad (2)$$

$$Selectivity_{\text{product}}\ (\%) = \frac{Yield_{\text{product}}}{Conversion_{\text{substrate}}} \cdot 100\% \qquad (3)$$

$$Mass\ balance\ (\%) = \frac{n_{\text{produced products}} + n_{\text{unreacted substrate}}}{n_{\text{starting substrate}}} \cdot 100\ \% \qquad (4)$$

where, n_x stands for the amount of the mentioned species in the equations (in mol), determined by HPLC analyses.

The conversion of fructose into HMF and furfural was monitored through the mass balance during the MW-assisted catalytic conversion. The formation of humins or soluble polymers can be visually identified by the coloration of the solutions. The mass balance provides semiquantitative information on the extent of humins formation.

3. Results and Discussion

3.1. Textural and surface properties by low-temperature nitrogen adsorption.

Figure 1(A) shows the N_2 adsorption-desorption isotherms of the *x*%Nb-MG and reference samples. The materials show type-IV (IUPAC) isotherms [48] characteristic of mesoporous materials with uniform porosity. The 1.8%Nb-MG, 2.8%Nb-MG, and Nb-SBA-15 samples show Type IV(a) isotherms, i.e., when the adsorption and desorption branches do not fully match. In contrast, $NbOPO_4$ displays a Type IV(b) isotherm corresponding to closely matching adsorption and desorption branches. Moreover, the uncalcined sample MG possesses an H1 hysteresis loop, characteristic of mesoporous materials with uniform cylindrical pores, which changes to H2(a) upon calcination at 500 °C or decoration with niobium (V) surface oxide after impregnation with $NbCl_5$ solution followed by calcination at 500 °C, attributed to the presence of pore-blocking species or narrowed pore necks [48]. The amorphous characteristic of glassy materials before and after calcination was confirmed by powder X-ray diffraction (XRD), presented in **Figure S4**, Supporting Information. In the last case, the change in the hysteresis loop can be

assigned to the niobium oxide occupying the mesopores. The samples isotherms show a stepper capillary condensation, indicating uniform pores, except for $NbOPO_4$.

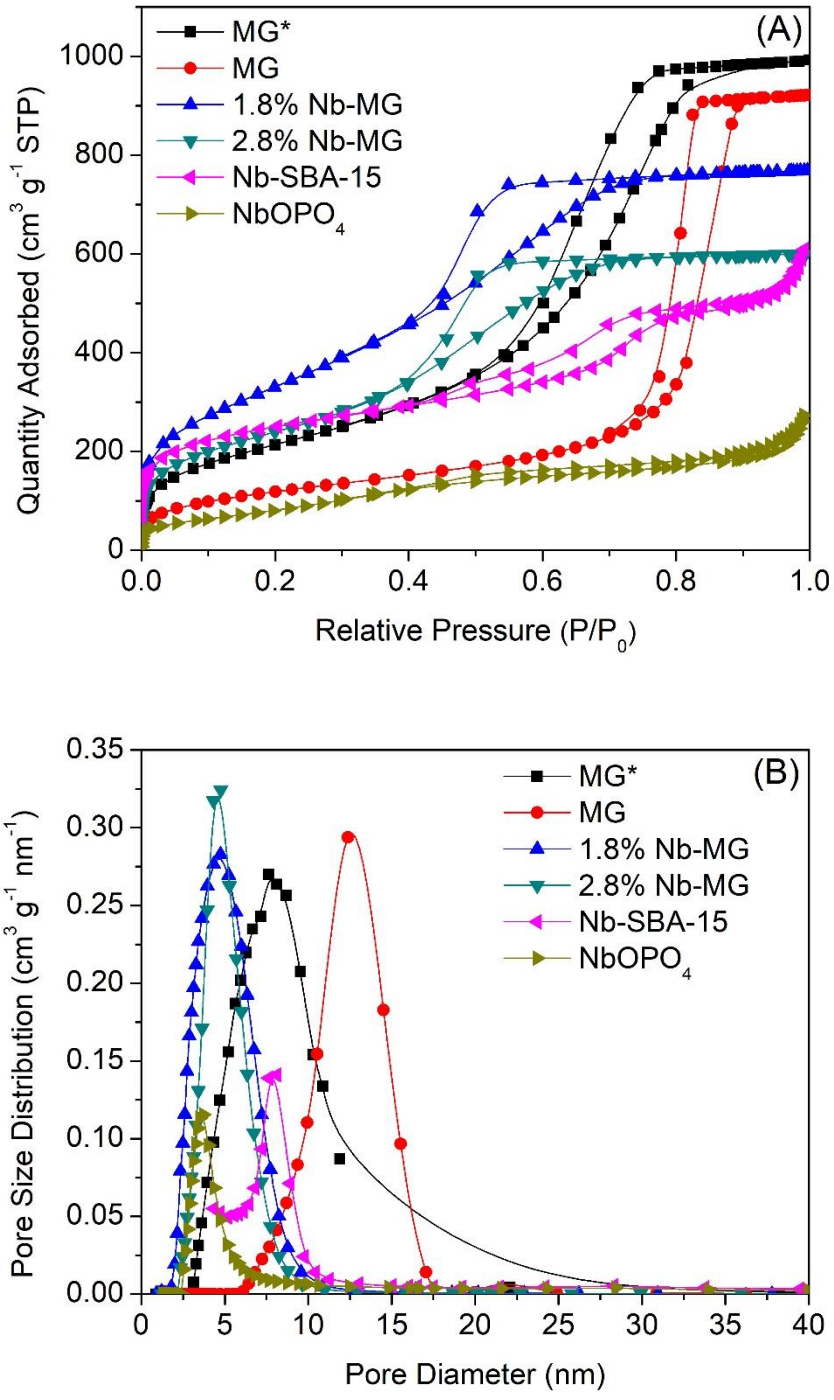

Figure 1. (A) N_2 adsorption-desorption isotherms, and (B) the corresponding pore size distributions for the niobium-oxide-containing mesoporous glasses (MG) and the reference materials. MG* indicates the uncalcined MG sample.

For the 1.8%Nb-MG, 2.8%Nb-MG, and Nb-SBA-15 samples, a small amount of N_2 adsorbed at low relative pressures (**Figure 1(A)**), which could be attributed to the presence of a small amount of microporosity (< 2 nm). This is generally expected for SBA-15 type materials [49] due to the P123 micelles connectivity during the self-assembly process [50]. However, α_s-plot analyses [48] identified no quantifiable microporosity (< 0.01 cm^3/g) for the glass-based materials (*x*%Nb-MG) and only ~0.04 cm^3/g of micropores in the Nb-SBA-15 material. The latter is two to three times smaller than expected for SBA-15 materials with similar surface area [49]. Thus, these observations indicate that the niobium oxide may have altered the surface structural characteristics of the SBA-15 support, enhancing its sintering during the calcination treatment. In the case of *x*%Nb-MG samples, the microporosity can be in the strangulated channels by Nb_2O_5 but insignificant in volume concentration, however, with a diameter detected by nitrogen adsorption.

The PSD curves (see **Figure 1(B)** [39]) of the *x*%Nb-MG and Nb-SBA-15 materials show peaks with maxima between 5 and 8 nm, confirming the materials' mesoporosity (2-50 nm). For comparison, their peak widths extend to the micropore range (< 2 nm), corroborating the presence of relatively 'large' micropores. In addition, the capillary condensation for the *x*%Nb-MG samples occurs at higher P/P_0 than in $NbOPO_4$ because of the larger pores of the first ones. The microstructural and morphological characteristics of the synthesized and reference materials are summarized in **Table 1**.

Considering the effect of thermal treatment alone (converting MG* into MG), the glass's pore volume and specific surface area decreased. At the same time, the mesopore modal diameter increased, as expected. This behavior is generally found in ceramic materials [28]. It can be characterized by a decrease in the number and

an increase in the size (coarsening) of grains and pores at the expense of the smaller ones, occurring simultaneously and concurrently with sintering. However, the presence of niobium chloride during the thermal treatment of the mesoporous glass support (MG) completely changed this phenomenon, generating materials with smaller pore volumes and sizes and higher specific surface areas. The former is expected upon post-synthesis impregnation. The latter is another indication of structural and surface modification of the glass support in the presence of the niobium compounds.

Table 1. Microstructural and morphological characteristics of samples under study.

Sample	V_t ($cm^3 \cdot g^{-1}$)[a]	S_{BET} ($m^2 \cdot g^{-1}$)[b]	w_{KJS} (nm)[c]
MG*	1.53	794	7.6
MG	1.42	437	12.3
1.8%Nb-MG	1.22	1224	4.7
2.8%Nb-MG	0.96	874	4.8
Nb-SBA-15	0.55	895	8.1
$NbOPO_4$	0.29	302	3.7

[a] Total pore volume, V_t, calculated from the amount of N_2 adsorbed at the P/P_0 = 0.98. [b] Specific surface area, S_{BET}, values obtained from adsorption data at 0.05 < P/P_0 < 0.2. [c] Pore size (w_{KJS}) obtained from the maxima of the pore size distribution (PSD) curves calculated by the KJS method [39]. MG* denotes the uncalcined sample.

Because of indications that niobium oxide impregnation changes the surface characteristics of the support, the surface interaction with adsorbed nitrogen was evaluated by comparing the surface coverage among different materials (**Figure 2**). The N_2-adsorption isotherms of **Figure 1(A)** were normalized by the maximum adsorbed N_2 quantity at the monolayer capacity, V/V_m, to obtain the surface coverage profiles. In this manner, N_2 interactions with the material's surface can be

evaluated at too low relative pressures; thus, the abscissa is presented in a logarithmic scale up to 0.1 P/P_0. For comparison, LiChrospher Si-1000, an amorphous mesoporous commercial silica gel, was included in **Figure 2** as a reference**.** The complete adsorption data used to calculate surface coverage of LiChrospher Si-1000 is reported elsewhere [51].

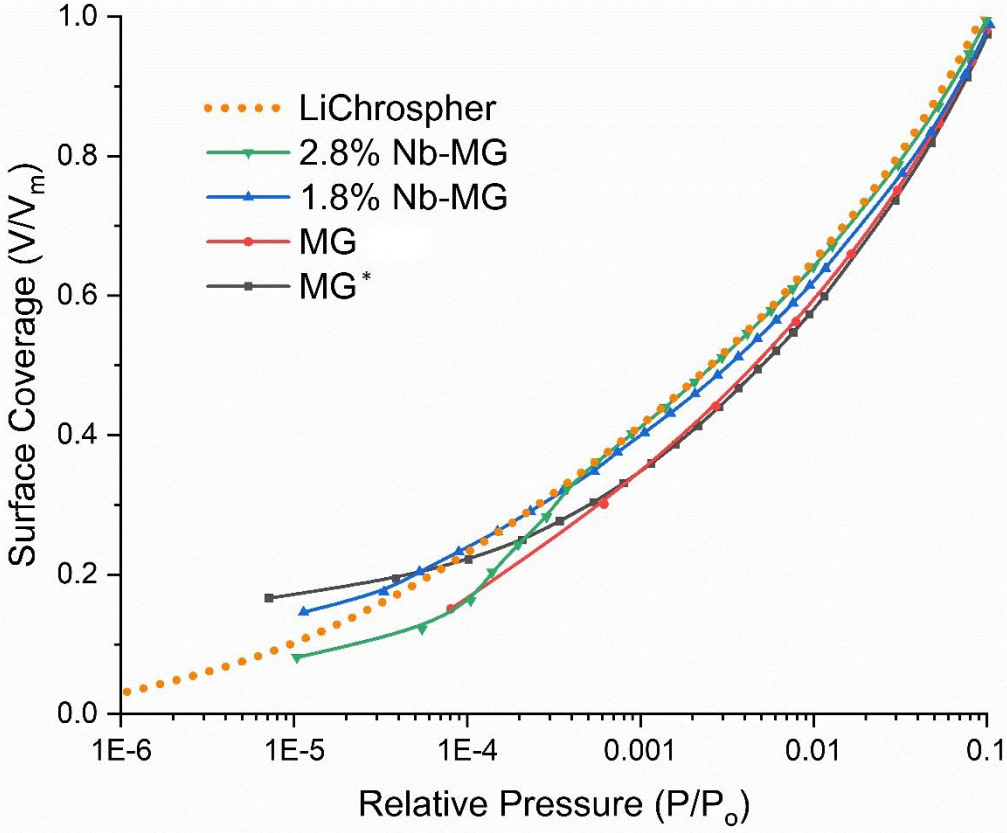

Figure 2. Surface adsorbed N_2 coverage curves for LiChrospher Si-1000 silica gel, mesopore glass supports, and *x*%Nb-MG samples.

It is well established that polar groups in silica-based materials (e.g., silanols groups: ≡Si-OH) increase nitrogen adsorption energy, consequently increasing low-pressure adsorption [52]. Comparing the reference mesoporous amorphous silica with MG* and MG samples, we notice the sol-gel derived glasses are less polar because of the smaller nitrogen adsorption occurring at $P/P_0 < 10^{-2}$ in **Figure 2**, corroborating our hypothesis that using glasses reduces the presence of silanol

groups. However, incorporating niobium oxide species on the MG surface, the presence of polar groups is reestablished, as indicated by the similarities among the profiles of 1.8%Nb-MG, 2.8%Nb-MG, and LiChrospher Si-1000 in the upper part of the low relative-pressure range in **Figure 2**. The same analysis is presented for all other samples in **Figure S5**, Supporting Information. All catalysts samples except Nb-SBA-15 presented similar surface properties to the LiChrospher Si-1000. Compared to this reference material, Nb-SBA-15 showed a higher surface coverage at very low relative pressures, most likely because of Nb-SBA-15 microporosity.

3.2. Surface Acidity

Figure 3 presents the ATR-FT-IR spectra of mesoporous silica glass support (MG), 1.8%Nb-MG, 2.8%Nb-MG, Nb-SBA-15, and $NbOPO_4$ samples before and after pyridine adsorption to distinguish the Brønsted and Lewis acid sites. The 1.8%Nb-MG, 2.8%Nb-MG, and Nb-SBA-15 samples showed absorption bands at 1447, 1490, 1545, and 1600 cm^{-1}, assigned to the pyridine vibration modes associated with acid sites [16]. The band at 1447 cm^{-1} is related to the interaction of pyridine with Lewis acid sites. The band at 1490 cm^{-1} is assigned to the interaction of pyridine with both Brønsted and Lewis acid sites. The band at 1545 cm^{-1} is associated with pyridinium ions produced by pyridine interaction with Brønsted acid sites. Finally, the 1600 cm^{-1} is assigned to H-bonded pyridine molecules interacting with bridged OH groups; this band is also related to the pyridine coordinated to Lewis acid sites (L). Moreover, the band at 1632 cm^{-1} is assigned to the H-O-H bending vibration of adsorbed water.

Figure 3 indicates that the MG presents negligible amounts of acid sites. The incorporation of Nb species creates both Lewis and Brønsted acid sites. However, the spectral data of pyridine adsorbed on the materials suggests that, with the

increase in Nb content, the creation of Brønsted acid sites seems to be slightly more predominant over Lewis acid sites. In turn, for $NbOPO_4$, Brønsted acid sites are present, while no significant amount of Lewis acid sites was found.

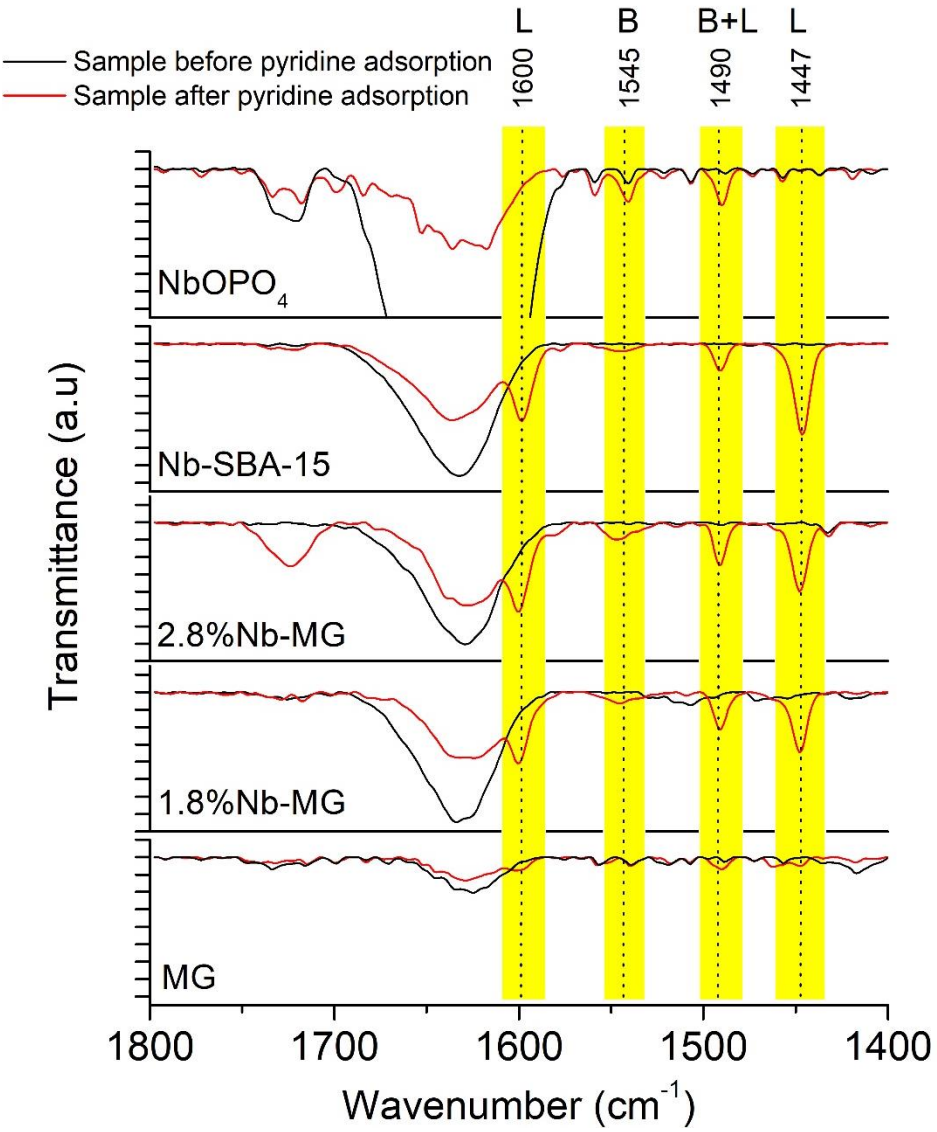

Figure 3. ATR-FT-IR spectra of catalyst samples studied before and after adsorption of pyridine.

Pyridine adsorption followed by non-isothermal desorption was monitored by thermogravimetry (TG) to assess the distribution of acid sites according to acid strength. The mass losses were used to calculate the acid site concentrations by a previously reported procedure [41–44], considering a 1:1 stoichiometry for pyridine

adsorption on the acid sites. The results are presented in **Table 2**. TG curves outline the pyridine desorption profile from the materials' acid sites (**Figure S6**, Supporting Information). The first mass loss event (30-100 °C) is attributed to both physisorbed pyridine and pyridine adsorbed on weakly acidic sites. The mass loss events between 100 to 300 °C and 300 to 550 °C are assigned to pyridine chemisorbed on medium and strong acid sites. Mass losses at higher temperatures are not discussed because they occur above the temperatures utilized to prepare the catalytic materials. They may be associated with further dehydration of the material's surface and occur during the sintering process. The obtained acidity values are similar to those of silica-based materials reported in the literature [53,54] and lower than those found for alumina-based materials or zeolites [28,50,53]. We found that the density of strong acid sites increases with Nb%, which correlates with an increased number of Lewis acid sites (as indicated by the FT-IR spectra of pyridine adsorbed on the materials, **Figure 3**). However, a clear correlation between Nb content and weak, medium, or total acid site density was not observed.

Table 2. Acidity profile of the synthesized materials determined by pyridine thermodesorption and Nb content (in wt%, as determined by ICP-OES).

Sample	Acid site density ($mmol \cdot m^{-2}$)[a]				Nb%
	Weak	Medium	Strong	Total	
MG	0.54	0.75	0.04	1.35	-
1.8%Nb-MG	0.22	0.40	0.09	0.72	1.5
2.8%Nb-MG	0.27	0.53	0.18	0.99	3.1
Nb-SBA-15	0.64	1.51	0.20	2.36	10.3
$NbOPO_4$	0.52	0.86	0.66	2.05	50.3

[a] Temperature ranges: weak and medium strength acid sites (T = 30-100 °C and 100-300 °C); strong acid sites (T = 300-550 °C).

3.3. Structural Characterization by Solid-State NMR

Figure 4 shows the ^{29}Si MAS NMR spectra. The lineshapes could consistently be fitted to three Gaussian components with essentially identical linewidths and chemical shifts between different samples, listed in **Table S1**, Supporting Information. The dominant component near -109 ppm is assigned to Si^4 units, engaged in four Si-O-Si linkages, an expected feature of the glass phase. In principle, the components at -99.9 and -90.8 ppm could reflect either Si^3 units having one and two terminal Si-OH groups, respectively, or Si^4 units featuring Si-O-Nb linkages; there could also be a combination of both structural elements.

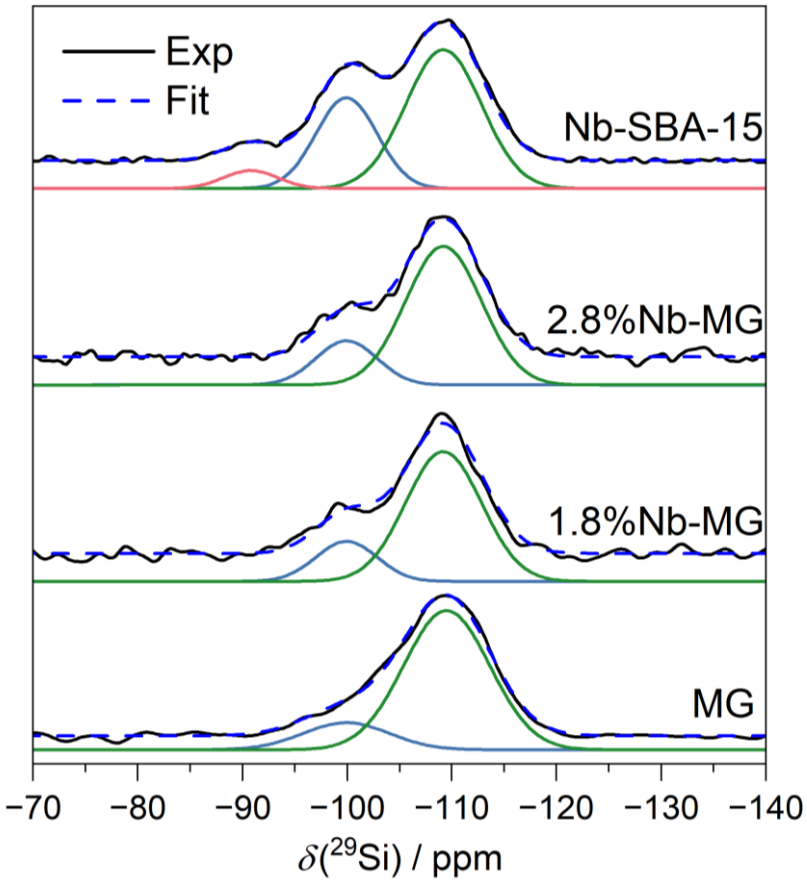

Figure 4. ^{29}Si MAS NMR spectra of samples under study. The dark blue dashed line indicates the sum of fits made up by the individual components (red, light blue, and green curves).

Previous ^{29}Si MAS-NMR experiments to identify the chemical shift of Si^4 units associated with the Si-O-Nb linking in SiO_2-Nb_2O_5 sol-gel materials were inconclusive, as the materials were prone to phase separation [55]. That study also examined the materials to identify whether the Si-O-Nb linking was present. Using a recently developed dipolar recoupling method involving saturation of the ^{93}Nb spin system via WURST pulses [56], no positive evidence of Si-O-Nb linking was obtained. On the other hand, this experiment also does not rule out their presence, so identifying the Si-O-Nb linking in these materials remains elusive. Nevertheless, the monotonic increase of the signal intensity near -99.9 ppm with increasing Nb content is consistent with forming some Nb-O-Si linkages at the surface. This is also supported by the characterization studies, which showed that Nb modified the surface of MG increasing its polarity. However, the materials possess high surface areas and low loading of Nb; thus, the surface modification would be noticeable only upon high dispersion of Nb species – arguing in favor of the formation of Nb-O-Si linkages.

Figure 5 shows static ^{93}Nb NMR spectra of all the Nb-containing samples. For clarity, only the central $m = ½ \leftrightarrow m = -½$ transitions are shown. The lineshapes reflect spectra likely dominated by second-order nuclear electric quadrupolar line broadening effects in a wide distribution of quadrupolar coupling parameters. Note that the ^{93}Nb NMR spectra from SBA-15 and the Nb-surface oxide decorating the internal surfaces of mesoporous silica glasses are different from that of bulk Nb_2O_5. This result indicates that the niobium oxide formed on the surface has a local structure different from bulk Nb_2O_5. **Table S2**, Supporting Information, lists the average isotropic chemical shifts $\langle\delta_{iso}\rangle$ and quadrupolar coupling parameters $\langle C_Q\rangle$ obtained when modeling the spectra with the Czjzek distribution [57]. The data are

comparable to values of six-coordinate niobium found in the literature [58–61], suggesting that the Nb-surface oxides have a similar local environment featuring six-coordinated Nb. Nevertheless, the different lineshapes observed for the 1.8%Nb-MG and the 2.8%Nb-MG suggest that the local structure of the Nb sites depends on the loading level. The local Nb structure of 2.8%Nb-MG seems quite similar to the Nb-SBA-15 material.

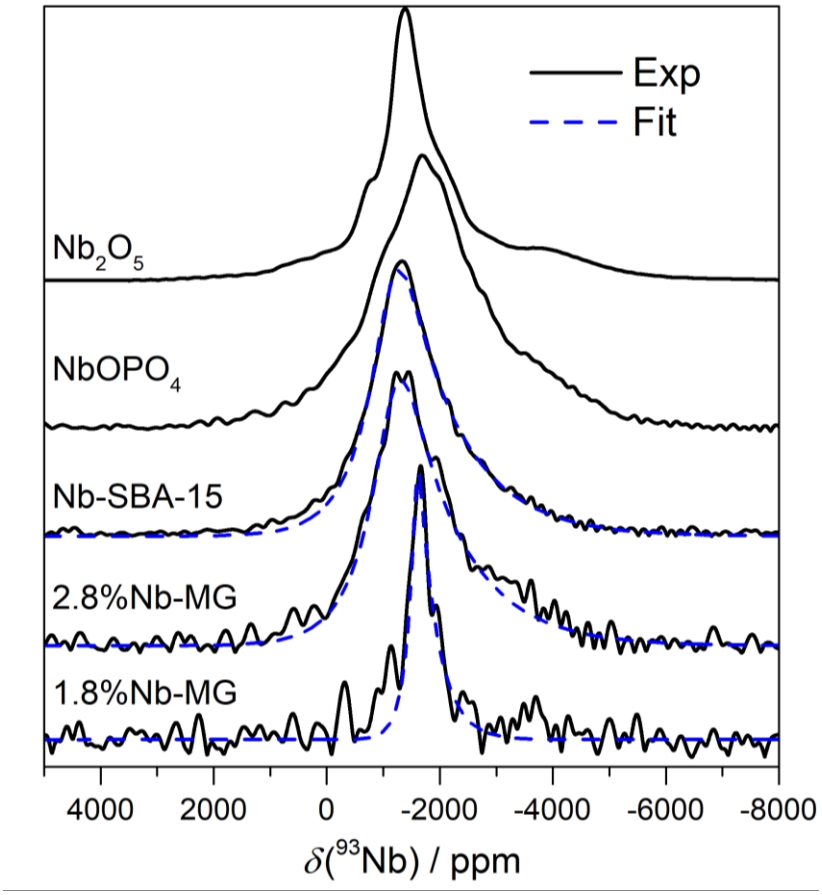

Figure 5. Static ^{93}Nb WCPMG NMR spectra of the samples under study, including Nb_2O_5 as reference material. Dashed curves indicate approximate lineshape fits based on the Czjzek model.

Figure 5 also includes a ^{93}Nb NMR spectrum of mesoporous $NbOPO_4$, again portraying a rather strongly disordered material. In this case, however, modeling the line shape by a single Czjzek distribution was unsuccessful. The resonance shift listed in **Table S2**, Supporting Information, comprises the isotropic chemical shift and

a second-order quadrupolar shift. For bulk crystalline $NbOPO_4$, (space group P_{nma}), the following lineshape parameters were previously determined: δ_{iso} = -1316 ppm, C_Q = 21 MHz, η_Q = 0.12 [61]. Finally, the spectrum of crystalline Nb_2O_5 looks rather complex and has, to date, not been satisfactorily analyzed partly due to several nonequivalent Nb sites [62]. In addition to the wideline NMR spectra, we also recorded MAS-NMR spectra at spinning speeds up to 60 kHz, resulting in rather low signal-to-noise spectra (data not shown), suggesting that only a small fraction of the Nb sites were detected in this manner. All these results indicate that the Nb(V) surface oxide sites are affected by very strong quadrupolar interactions with a wide distribution of tensor parameters.

3.4. Conversion of hexoses to HMF in a biphasic reaction system

Biphasic reaction systems have extensively been demonstrated as an efficient strategy to reduce the degradation of furfurals to humins [9,18,19]. To verify the potential of Nb-containing materials in the conversion of hexoses to HMF, we chose to perform the reaction in a biphasic reaction system assisted by microwave heating. In the biphasic system, fructose dissolved in brine solution undergoes dehydration rendering HMF. At the same time, HMF is extracted from the aqueous phase to the organic phase (methyl isobutyl ketone) [63–65]. **Figure 6** and **Table 3** summarize the results obtained at 170 °C and a reaction time of 8 min, obtained with catalyst loadings of 10 and 20 mg.

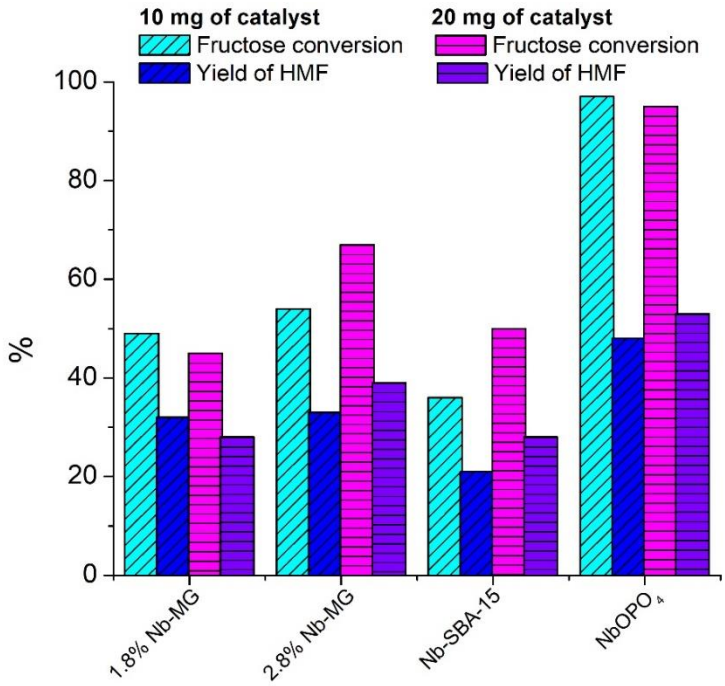

Figure 6. Comparison of values of fructose conversion and HMF yield obtained from the microwave-assisted dehydration of fructose performed in a biphasic reaction system. Reaction conditions: fructose (0.1 mmol), catalyst (10 mg or 20 mg), 8 min, microwave heating at 170 °C.

Table 3. Results of microwave-assisted dehydration of fructose in the presence of niobium-containing materials in a biphasic reaction system[a]

Sample	Cat. weight (mg)	Fructose conversion (%)[b]	HMF yield (%)[c]	HMF selectivity (%)[d]	Mass balance (%)[e]	HMF productivity (g_{HMF}/g_{Nb})
1.8%Nb-MG	10	49	32	65	83	26.9
2.8%Nb-MG		54	33	61	79	13.4
Nb-SBA-15		36	21	58	85	2.5
$NbOPO_4$		97	48	49	51	1.2
MG* (control)	20	5	1	20	96	0
1.8%Nb-MG		45	28	62	83	11.7
2.8%Nb-MG		67	39	58	72	7.9
Nb-SBA-15		50	28	56	78	1.7
$NbOPO_4$		95	53	56	58	0.6

*Thermal conversion, studied in the presence of the uncalcined MG support. [a] Reaction conditions: fructose (0.1 mmol), catalyst (10 mg or 20 mg), 8 min, microwave heating at 170 °C. [b] Eq 1. [c] Eq 2. [d] Eq 3. [e] Eq 4.

The control experiment performed in the presence of Nb-unloaded MG material (20 mg) resulted in a very low conversion of fructose (5%) into a negligible amount of HMF (obtained at a 1% yield). At the low catalyst loading (10 mg), good conversions of fructose (49-54%) into HMF (at yields of 32-33%), in the presence of 1.8%Nb-MG and 2.8%Nb-MG, were achieved. In contrast, the reaction in the presence of Nb-SBA-15 presented a low conversion of fructose (36%), yielding 21% of HMF. Finally, almost quantitative conversion of fructose (97%) was achieved in the presence of $NbOPO_4$, rendering a 48% yield of HMF. As listed in **Table 3**, the increase in catalyst loading (from 10 to 20 mg) improved fructose conversion and HMF yield for the experiments carried out with Nb-SBA-15 and 2.8%Nb-MG. However, a marginal effect was observed in the experiments performed in the presence of 1.8%Nb-MG. Unsurprisingly, the results obtained for experiments in the presence of $NbOPO_4$ were similar regardless of the catalyst loading, corroborating the high activity found for this material.

Table 3 shows the HMF productivity for the synthesized catalysts, defined as grams of HMF produced per grams of Nb in the catalyst composition. For both catalyst loadings (10 mg or 20 mg), 1.8%Nb-MG and 2.8%Nb-MG catalysts present productivities significantly higher, compared to the other tested materials. This indicates that the high degree of Nb dispersion onto the support improves the utilization of Nb(V) species since they are grafted on the surface of MG. In $NbOPO_4$, a less atom economic utilization of Nb is caused by Nb(V) species being present on both the surface and in the structure. The latter are more significant in number than the former Nb(V) species. However, the Nb(V) structural sites not exposed to the surface are inactive for the dehydration of fructose to HMF. Interestingly, HMF productivities for all Nb-containing materials dropped by about 40-50% when the

catalyst loading was increased (from 10 mg to 20 mg). Once again, this observation suggests that Nb materials present high activities for both converting fructose into HMF and forming humins from HMF and fructose. As the formation of humins seems to be a very fast reaction in the aqueous phase, the formation of humins is only partially mitigated by using the biphasic reaction system.

To further understand the surface chemistry features of niobium-containing materials, we explored the materials for converting glucose to HMF under the similar reaction conditions used for the fructose conversion. **Table 4** summarizes the results obtained from the conversion of glucose. Low conversion of glucose was achieved for all materials, while 2.8%Nb-MG was inactive for the conversion of glucose. The modest performance of 1.8%Nb-MG, Nb-SBA-15, $NbOPO_4$ in the dehydration of glucose into HMF indicates that the materials present a low activity for the isomerization of glucose into fructose.

Table 4. Results of conversion of glucose catalyzed by *x*%Nb-MG catalysts under MW irradiation in a monophasic reaction system[a]

Sample	Glucose conversion (%)[b]	Fructose Yield (%)	HMF Yield (%)[c]	Furfural Yield (%)	Mass balance (%)[d]
blank	10	7	0	0	97
1.8%Nb-MG	11	0	7	0	96
2.8%Nb-MG	0	0	0	0	100
Nb-SBA-15	16	0	9	0	93
$NbOPO_4$	29	0	18	0	89

[a] Reaction conditions: 18 mg of the substrate, 20 mg of catalyst, 4 min, 170 °C. [b] Eq 1. [c] Eq 2. [d] Eq 4.

Nakajima *et al.* highlighted that a large amount of Nb is needed to promote the conversion of glucose to HMF [66]. Indeed, they have used an Nb_2O_5-to-glucose

weight ratio of 10:1 to achieve 90-100% conversion. In this study, we employed a catalyst-to-glucose (or fructose) ratio of 1:1. Moreover, the catalytic results shown in **Table 4** could indicate the lack of specific Lewis sites needed for the isomerization of glucose to fructose. However, the ATR-FT-IR studies confirmed the presence of Lewis acid sites (**Figure 3**). One could argue that the interaction with water eliminates most Lewis acid sites. Water can coordinate on the Lewis acid sites, and the hydrated species undergo partial hydrolysis, thus losing their activity as Lewis acid sites [67]. Unlike several Nb-containing materials, which have been demonstrated to be Lewis acid water-tolerant catalysts [66], the current materials might not present such a feature.

A survey on results obtained from the catalytic conversion of fructose and glucose into HMF using Nb-based catalysts is presented in **Table S3**, Supporting Information [9,18–26]. Although the reaction medium varies among the reported studies in the literature, some essential points can be highlighted: (i) the reaction time is significantly shorter when a microwave-assisted reaction is used, (ii) the Nb%-MG materials contain considerably lower levels of Nb than those investigated in any other study, (iii) although the conversion levels for Nb%-MG are lower than those obtained in other studies, the yields of HMF are comparable or higher, indicating a lower degree of byproduct formation, which is highly desirable. For instance, Antonetti et al. [24] performed microwave-assisted dehydration of fructose into HMF catalyzed by niobium phosphate catalyst under similar reaction conditions obtaining 97% conversion of fructose and yielding 32% HMF. For comparison, the Nb%-MG materials possess similar or higher yields of HMF, the product of interest.

It has been established that specific acid sites strongly influence the activity and selectivity of Nb-based catalysts for HMF production. Specifically, Lewis acid

sites are responsible for the isomerization of glucose to fructose, whereas Brønsted acid sites promote the conversion of fructose to HMF and humin [9]. Considering the data presented in **Figure 7(A)** and Nb-loading in the materials (See **Table 2**), the increase in Nb-loading is followed by the rise in both the density of Lewis acid sites and strong acid sites. To better understand this correlation, **Figure 7(A)** illustrates that the fructose conversion and the HMF yield correlate with the density of strong acid sites among the various catalysts studied – the higher the density of strong acid sites, the higher the fructose conversion or yield to HMF. Such correlation is not found for the density of weak and total acid sites, displayed in **Figure S7**, Supporting Information. The latter effect may be related to the different local environments seen in the ^{93}Nb NMR spectrum. Future investigation is needed to address this working hypothesis.

The correlation of catalytic results with the density of strong acid sites (**Figure 7(A)**) estimated by pyridine desorption seems to be related to the fact that Lewis acid sites polarize water creating weak Brønsted acid sites needed for the conversion of fructose to HMF [66]. Moreover, humins are formed when strong Lewis acid sites are present, which will always be the case for our catalysts because of the chemical equilibrium: LA + H_2O ⇌ [LA-OH_2], in which LA represents a Lewis acid site. Note that the hydration of Lewis acid sites is an equilibrium reaction and microwave heating is selective to water. Therefore, some Lewis acid sites may still be present under the reaction conditions. The highest selectivity was found for the catalyst with the lowest ratio of Lewis acid sites (1.8%Nb-MG), suggesting a favorable balance between Lewis and Brønsted acid sites compared to the other tested materials.

A strong correlation is observed when conversion is plotted against the unaccounted mass (100 - % mass balance), which is associated with humins

formation (**Figure 7(B)**). This is interesting considering the very distinct surface features and acid properties among all synthesized samples. Therefore, the materials cannot be clearly distinguished by different populations of acid site types. Nevertheless, regardless of the material employed as a catalyst, the formation of humins remained associated with the yield of HMF (even in a biphasic system). The presence of water and ion-exchange effects might level out the acid strength on the catalyst surface, thus creating an additional layer of complexity in understanding the acid properties (from pyridine adsorption experiments) and their impact on the catalyst performance in the dehydration of fructose and on the control over side reactions.

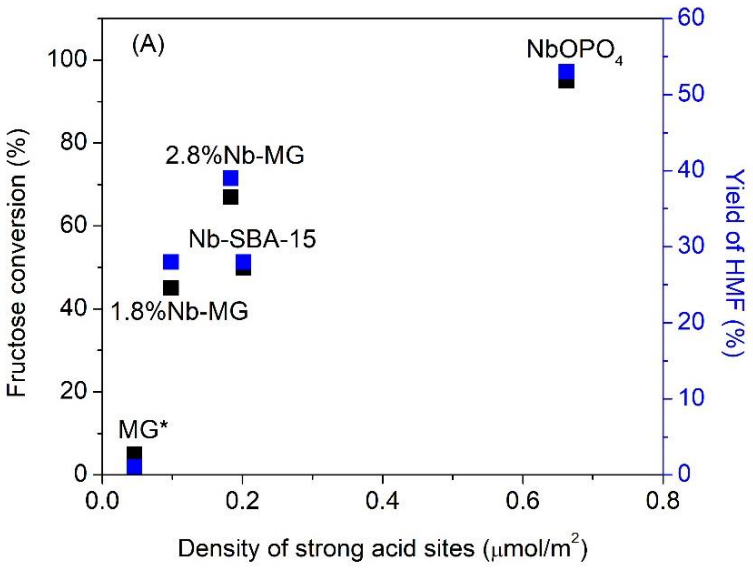

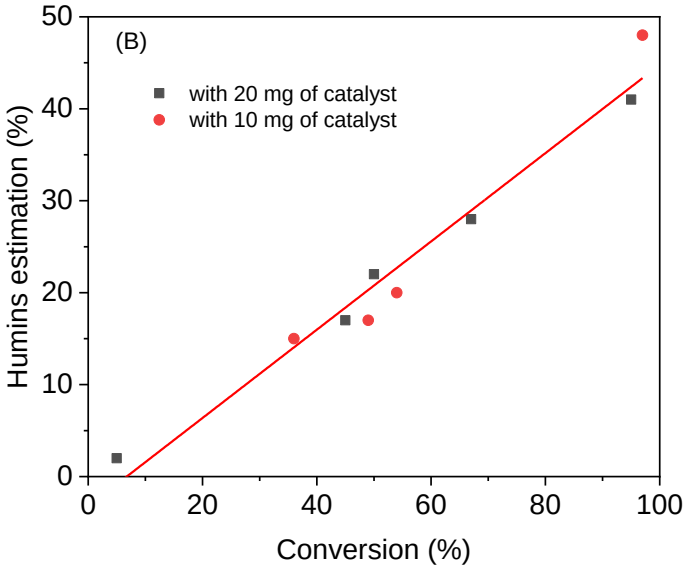

Figure 7. (A) Correlation between fructose conversion (or HMF yield) and the density of strong acid sites; (B) Correlation between fructose conversion and level of humin formation (estimated as 100 - % mass balance) – R^2 = 0.9648.

For a better insight into the catalytic performance of the Nb-containing glass catalysts, **Figure 8** compares the results herein obtained with the literature review presented in **Table S3**, Supporting Information. In a plot of HMF yield versus fructose conversion, the values close to the diagonal line represent the materials with high selectivity to HMF. Interestingly, the Nb-containing mesoporous glasses displayed the highest selectivity to HMF, apart from two exceptions. These exceptions are the catalysts presented by Yang et al. [19] and Ngee et al. [20]. However, these results were not obtained with similar catalysts as those described herein. When using Nb_2O_5-H_3PO_4 as a catalyst [19], both Lewis acid sites (related to NbO_x surface species) and Brønsted acid sites (related to H_3PO_4 surface species) are present. Therefore, supporting H_3PO_4 overcomes the limitation seen in this study in which the catalysts mostly present Lewis acid sites. In addition, the authors employed water as the medium phase instead of brine, as the reaction using brine

results in ion exchange, deactivating any Brønsted acid site. The second result closest to the diagonal line was obtained performing the reaction in DMSO, where solvation effects contribute to improved yield. However, this solvent is not a suitable reaction medium for this process.

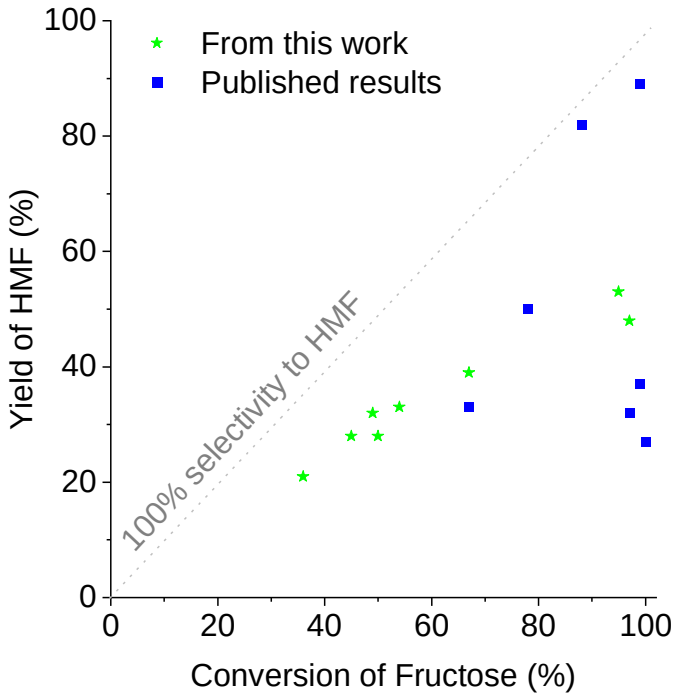

Figure 8. HMF yields as a function of fructose conversion obtained from this work and its comparison with literature results.

Furthermore, **Figure 9** illustrates that the extent of humin formation, as visually indicated by the coloration of the solution, is significantly lower than for the reference materials. For comparison, **Figure S8**, Supporting Information, displays the coloration in cases where a catalyst leads to the high formation of humins. This is also supported by the HMF selectivity values displayed in **Table 3**.

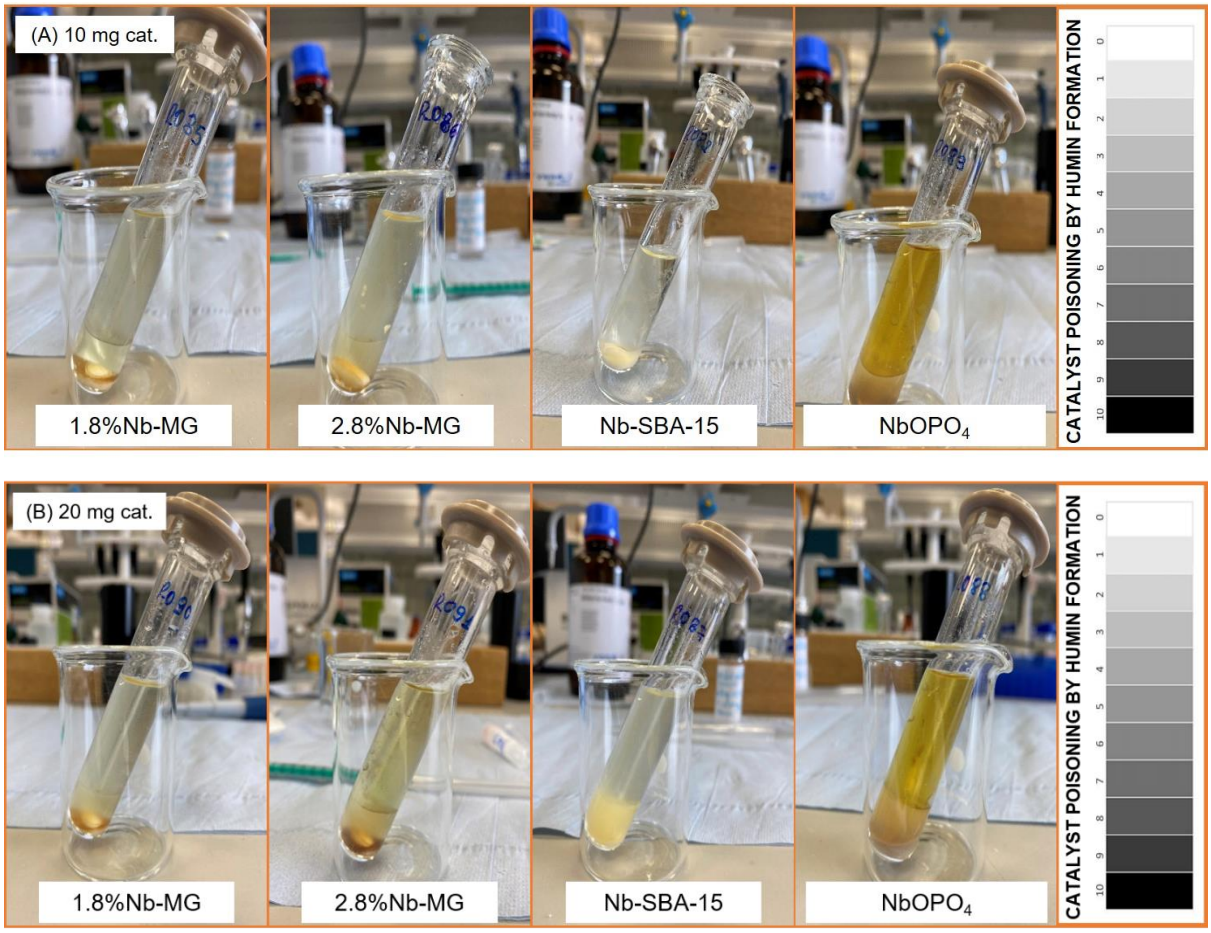

Figure 9. Lower levels of humin formation (less strongly colored solutions) were observed for the dehydration of fructose into HMF by the *x*%Nb-MG catalysts and in Nb-SBA-15.

The main advantage of our synthesis strategy is the production of a highly dispersed Nb surface oxide on the internal surfaces of the mesoporous glass, which allows one to utilize very low levels of Nb content. This feature was demonstrated to be conducive to high productivity of HMF (Table 3). Consequently, the present study results suggest that it may be possible to tailor the fraction of Lewis acid sites to maximize HMF selectivity for fructose-specific conditions. Nonetheless, humins formation also correlates with the degree of conversion and not the type of acid sites, indicating that process conditions should maximize HMF yield at a suitable conversion level to obtain optimal mass balance. Such a strategy can potentially

minimize humins formation and catalyst deactivation. This idea is further supported by the results presented in **Table S3**, Supporting Information, and **Figure 8,** comparing the synthesized catalysts' conversion and HMF yield and selectivity with data reported in the literature.

4. Conclusion

Mesoporous silica glasses decorated with surface niobium oxide are very active catalysts for converting fructose into HMF under mild conditions. The fast conversion of fructose into HMF is attributed to the high dispersion of niobium surface oxide on the internal surface of the mesoporous glass. Using a highly porous glass matrix allowed much better utilization of niobium atoms, compared to Nb-SBA-15 and $NbOPO_4$. The improved dispersion of Nb leads to high HMF productivity. For the highly porous niobium-containing glasses, the HMF productivity was about 10 to 20-times higher than that achieved in the presence of $NbOPO_4$ in the experiments with a low catalyst loading. The high dispersion of Nb was achieved due to the glass support's large surface area combined with a low loading of Nb forms Si-O-Nb environments, allowed for the generation of varied densities of Lewis and Brønsted acid sites.

The role of Lewis and Brønsted acid sites on niobium-containing glasses' surface in the formation mechanism of HMF and humins remain elusive. In the catalytic process, the strong Brønsted acid sites most likely undergo ion exchange in the brine phase of the biphasic reaction system to convert fructose to HMF. Therefore, we propose that Lewis acid sites indirectly govern the catalytic activity since a part of the Lewis acid site population and water react, forming weak Brønsted acid sites. These sites are expected to be more 'resistant' towards ion-

exchange under reaction conditions, remaining active for fructose dehydration into HMF. However, some of the remnant Lewis acid sites may be water-resistant and, thus, involved in the formation of humins. Therefore, this study also highlights the timely need for further in-situ studies to unveil the complexity of the interface between the solid acid catalyst's surface and the brine solution containing fructose and 'just-formed' HMF, to further the understanding of the role of the Nb sites in the conversion of fructose to HMF.

Authors, contribution

Maria J. F. Costa: Conceptualization, Methodology, Investigation, Formal Analysis, Writing – original draft. **Alexandre A. S. Gonçalves:** Methodology, Investigation, Writing – original draft. **Roberto Rinaldi:** Conceptualization, Investigation, Writing – original draft, Supervision, Funding acquisition. **Henrik Bradtmüller:** Methodology, Investigation, Formal Analysis, Writing – original draft. **Hellmut Eckert:** Conceptualization, Writing – original draft, Supervision, Project administration, Funding acquisition. **Eduardo B. Ferreira:** Conceptualization, Writing – original draft, Supervision, Project administration, Funding acquisition.

Competing interests

The authors declare no competing interests.

Declaration of interests

The authors declare that they have no known competing financial interests or personal relationships that could have influenced the work reported in this paper.

Acknowledgments

This work was supported by the São Paulo Research Foundation (FAPESP - Brazil), through the Center for Research, Technology, and Education in Vitreous Materials (CeRTEV), grant No. 2013/07793-6. M.J.F.C. thanks FAPESP for postdoctoral fellowships with grants No. 2016/14165-0 and 2019/12884-7. A.A.S.G. collaborated as an independent researcher and acknowledges the National Council for Scientific and Technological Development (CNPq - Brazil) grant No. 200511/2012-2. H.B. also acknowledges the support from the FAPESP with grant No. 2019/26399-3. R.R. acknowledges the financial support by ERC Consolidator Grant “Ligninfirst” (Grant agreement ID: 725762).

References

[1] L.A.B. Cortez, Bioetanol de cana-de-açúcar, FAPESP, São Paulo, 2010.

[2] G.W. Huber, S. Iborra, A. Corma, Synthesis of transportation fuels from biomass: Chemistry, catalysts, and engineering, Chem. Rev. 106 (2006) 4044–4098. https://doi.org/10.1021/cr068360d.

[3] R. Rinaldi, F. Schüth, Design of solid catalysts for the conversion of biomass, Energy Environ. Sci. 2 (2009) 610–626. https://doi.org/10.1039/b902668a.

[4] C.O. Tuck, E. Pérez, I.T. Horváth, R.A. Sheldon, M. Poliakoff, Valorization of biomass: Deriving more value from waste, Science. 337 (2012) 695–699. https://doi.org/10.1126/science.1218930.

[5] O. Casanova, S. Iborra, A. Corma, Biomass into chemicals: Aerobic oxidation of 5-hydroxymethyl-2-furfural into 2,5-furandicarboxylic acid with gold nanoparticle catalysts, ChemSusChem. 2 (2009) 1138–1144. https://doi.org/10.1002/cssc.200900137.

[6] X. Tong, Y. Ma, Y. Li, Biomass into chemicals: Conversion of sugars to furan derivatives by catalytic processes, Appl. Catal. A Gen. 385 (2010) 1–13. https://doi.org/10.1016/j.apcata.2010.06.049.

[7] J. Zhang, L. Lin, S. Liu, Efficient production of furan derivatives from a sugar mixture by catalytic process, Energy and Fuels. 26 (2012) 4560–4567. https://doi.org/10.1021/ef300606v.

[8] H. Xiong, H.N. Pham, A.K. Datye, Hydrothermally stable heterogeneous catalysts for conversion of biorenewables, Green Chem. 16 (2014) 4627–4643. https://doi.org/10.1039/c4gc01152j.

[9] Y. Zhang, J. Wang, X. Li, X. Liu, Y. Xia, B. Hu, G. Lu, Y. Wang, Direct conversion of biomass-derived carbohydrates to 5-hydroxymethylfurural over

water-tolerant niobium-based catalysts, Fuel. 139 (2015) 301–307. https://doi.org/10.1016/j.fuel.2014.08.047.

[10] J.C. Serrano-Ruiz, R.M. West, J.A. Dumesic, Catalytic conversion of renewable biomass resources to fuels and chemicals, Annu. Rev. Chem. Biomol. Eng. 1 (2010) 79–100. https://doi.org/10.1146/annurev-chembioeng-073009-100935.

[11] C.-H.H. Zhou, X. Xia, C.-X.X. Lin, D.-S.S. Tong, J. Beltramini, Catalytic conversion of lignocellulosic biomass to fine chemicals and fuels, Chem. Soc. Rev. 40 (2011) 5588. https://doi.org/10.1039/c1cs15124j.

[12] D.K. Ratnasari, W. Yang, P.G. Jönsson, Kinetic study of an H-ZSM-5/Al-MCM-41 catalyst mixture and its application in lignocellulose biomass pyrolysis, Energy and Fuels. 33 (2019) 5360–5367. https://doi.org/10.1021/acs.energyfuels.9b00866.

[13] A. Osatiashtiani, A.F. Lee, M. Granollers, D.R. Brown, L. Olivi, G. Morales, J.A. Melero, K. Wilson, Hydrothermally Stable, Conformal, Sulfated Zirconia Monolayer Catalysts for Glucose Conversion to 5-HMF, ACS Catal. 5 (2015) 4345–4352. https://doi.org/10.1021/acscatal.5b00965.

[14] C.A.S. Lanziano, S.F. Moya, D.H. Barrett, E. Teixeira-Neto, R. Guirardello, F.S. Silva, R. Rinaldi, C.B. Rodella, Hybrid-organic-inorganic anatase as a bifunctional catalyst for enhanced production of HMF from glucose in water, ChemSusChem. (2018) 872 – 880. https://doi.org/10.1002/cssc.201702354.

[15] X. Li, Y. Zhang, The conversion of 5-hydroxymethyl furfural (HMF) to maleic anhydride with vanadium-based heterogeneous catalysts, Green Chem. 18 (2016) 643–647. https://doi.org/10.1039/c5gc01794g.

[16] G.F. Leal, S. Lima, I. Graça, H. Carrer, D.H. Barrett, E. Teixeira-Neto, A.A.S.

Curvelo, C.B. Rodella, R. Rinaldi, Design of Nickel Supported on Water-Tolerant Nb_2O_5 Catalysts for the Hydrotreating of Lignin Streams Obtained from Lignin-First Biorefining, IScience. 15 (2019) 467–488. https://doi.org/10.1016/j.isci.2019.05.007.

[17] F.L. Grasset, B. Katryniok, S. Paul, V. Nardello-Rataj, M. Pera-Titus, J.M. Clacens, F. De Campo, F. Dumeignil, Selective oxidation of 5-hydroxymethylfurfural to 2,5-diformylfuran over intercalated vanadium phosphate oxides, RSC Adv. 3 (2013) 9942–9948. https://doi.org/10.1039/c3ra41890a.

[18] G. Qiu, C. Huang, X. Sun, B. Chen, Highly active niobium-loaded montmorillonite catalysts for the production of 5-hydroxymethylfurfural from glucose, Green Chem. 21 (2019) 3930–3939. https://doi.org/10.1039/c9gc01225g.

[19] F. Yang, Q. Liu, X. Bai, Y. Du, Conversion of biomass into 5-hydroxymethylfurfural using solid acid catalyst, Bioresour. Technol. 102 (2011) 3424–3429. https://doi.org/10.1016/j.biortech.2010.10.023.

[20] E.L.S. Ngee, Y. Gao, X. Chen, T.M. Lee, Z. Hu, D. Zhao, N. Yan, Sulfated Mesoporous Niobium Oxide Catalyzed 5-Hydroxymethylfurfural Formation from Sugars, Ind. Eng. Chem. Res. 53 (2014) 14225–14233. https://doi.org/10.1021/ie501980t.

[21] H. Jiao, X. Zhao, C. Lv, Y. Wang, D. Yang, Z. Li, X. Yao, Nb_2O_5-γ-Al_2O_3 nanofibers as heterogeneous catalysts for efficient conversion of glucose to 5-hydroxymethylfurfural, Sci. Rep. 6 (2016). https://doi.org/10.1038/srep34068.

[22] C. Yue, G. Li, E.A. Pidko, J.J. Wiesfeld, M. Rigutto, E.J.M. Hensen, Dehydration of Glucose to 5-Hydroxymethylfurfural Using Nb-doped Tungstite,

ChemSusChem. 9 (2016) 2421-2429. https://doi.org/10.1002/cssc.201600649.

[23] E.G.L. de Carvalho, F. de A. Rodrigues, R.S. Monteiro, R.M. Ribas, M.J. da Silva, Experimental design and economic analysis of 5-hydroxymethylfurfural synthesis from fructose in acetone-water system using niobium phosphate as catalyst, Biomass Convers. Biorefinery. 8 (2018) 635–646. https://doi.org/10.1007/s13399-018-0319-5.

[24] C. Antonetti, M. Melloni, D. Licursi, S. Fulignati, E. Ribechini, S. Rivas, J.C. Parajó, F. Cavani, A.M. Raspolli Galletti, Microwave-assisted dehydration of fructose and inulin to HMF catalyzed by niobium and zirconium phosphate catalysts, Appl. Catal. B Environ. 206 (2017) 364–377. https://doi.org/10.1016/j.apcatb.2017.01.056.

[25] M.N. Catrinck, E.S. Ribeiro, R.S. Monteiro, R.M. Ribas, M.H.P. Barbosa, R.F. Teófilo, Direct conversion of glucose to 5-hydroxymethylfurfural using a mixture of niobic acid and niobium phosphate as a solid acid catalyst, Fuel. 210 (2017) 67–74. https://doi.org/10.1016/j.fuel.2017.08.035.

[26] K. Peng, X. Li, X. Liu, Y. Wang, Hydrothermally stable Nb-SBA-15 catalysts applied in carbohydrate conversion to 5-hydroxymethyl furfural, Mol. Catal. 441 (2017) 72–80. https://doi.org/10.1016/j.mcat.2017.04.034.

[27] K.T. Jacob, C. Shekhar, M. Vinay, Y. Waseda, Thermodynamic properties of niobium oxides, J. Chem. Eng. Data. 55 (2010) 4854–4863. https://doi.org/10.1021/je1004609.

[28] A.A.S. Gonçalves, M.J.F. Costa, L. Zhang, F. Ciesielczyk, M. Jaroniec, One-Pot Synthesis of $MeAl_2O_4$ (Me = Ni, Co, or Cu) Supported on γ-Al_2O_3 with Ultralarge Mesopores: Enhancing Interfacial Defects in γ-Al_2O_3 To Facilitate the Formation of Spinel Structures at Lower Temperatures, Chem. Mater. 30

(2018) 436–446. https://doi.org/10.1021/acs.chemmater.7b04353.

[29] C. García-Sancho, R.M.A. Saboya, J.A. Cecilia, A. V. Sales, F.M.T. Luna, E. Rodríguez-Castellón, C.L. Cavalcante, Influence of pore size and loading for Nb2O5/SBA-15 catalysts on synthetic ester production from free fatty acids of castor oil, Mol. Catal. 436 (2017) 267–275. https://doi.org/10.1016/j.mcat.2017.04.036.

[30] T. Kitano, T. Shishido, K. Teramura, T. Tanaka, Brønsted Acid Property of Alumina-Supported Niobium Oxide Calcined at High Temperatures: Characterization by Acid-Catalyzed Reactions and Spectroscopic Methods, J. Phys. Chem. C. 116 (2012) 11615–11625. https://doi.org/10.1021/jp3032429.

[31] A.A.S. Gonçalves, P.B. Faustino, J.M. Assaf, M. Jaroniec, One-Pot Synthesis of Mesoporous Ni–Ti–Al Ternary Oxides: Highly Active and Selective Catalysts for Steam Reforming of Ethanol, ACS Appl. Mater. Interfaces. 9 (2017). https://doi.org/10.1021/acsami.6b15507.

[32] H.B. Zhang, G.G. Liu, L. Shi, J.H. Ye, Single-atom catalysts: Emerging multifunctional materials in heterogeneous catalysis, Adv. Energy Mater. 8 (2018). https://doi.org/10.1002/aenm.201701343.

[33] A.A.S. Gonçalves, F. Ciesielczyk, B. Samojeden, M. Jaroniec, Toward development of single-atom ceramic catalysts for selective catalytic reduction of NO with NH_3, J. Hazard. Mater. 401 (2021) 123413. https://doi.org/10.1016/j.jhazmat.2020.123413.

[34] Z. Xu, Y. Yang, P. Yan, Z. Xia, X. Liu, Z.C. Zhang, Mechanistic understanding of humin formation in the conversion of glucose and fructose to 5-hydroxymethylfurfural in [BMIM]Cl ionic liquid, RSC Adv. 10 (2020) 34732–34737. https://doi.org/10.1039/d0ra05641c.

[35] T.B. De Queiroz, M.B.S. Botelho, L. De Boni, H. Eckert, A.S.S. De Camargo, Strategies for reducing dye aggregation in luminescent host-guest systems: Rhodamine 6G incorporated in new mesoporous sol-gel hosts, J. Appl. Phys. 113 (2013). https://doi.org/10.1063/1.4795506.

[36] Y.M. Liu, Y. Cao, N. Yi, W.L. Feng, W.L. Dai, S.R. Yan, H.Y. He, K.N. Fan, Vanadium oxide supported on mesoporous SBA-15 as highly selective catalysts in the oxidative dehydrogenation of propane, J. Catal. 224 (2004) 417–428. https://doi.org/10.1016/j.jcat.2004.03.010.

[37] M. Trejda, A. Tuel, J. Kujawa, B. Kilos, M. Ziolek, Niobium rich SBA-15 materials - preparation, characterisation and catalytic activity, Microporous Mesoporous Mater. 110 (2008) 271–278. https://doi.org/10.1016/j.micromeso.2007.06.015.

[38] A. Sarkar, P. Pramanik, Synthesis of mesoporous niobium oxophosphate using niobium tartrate precursor by soft templating method, Microporous Mesoporous Mater. 117 (2009) 580–585. https://doi.org/10.1016/j.micromeso.2008.08.001.

[39] M. Jaroniec, L.A. Solovyov, Improvement of the Kruk-Jaroniec-Sayari method for pore size analysis of ordered silicas with cylindrical mesopores, Langmuir. 22 (2006) 6757. https://doi.org/10.1021/la0609571.

[40] F.C.F. Marcos, J.M. Assaf, R. Giudici, E.M. Assaf, Surface interaction of CO_2/H_2 mixture on mesoporous ZrO_2: Effect of crystalline polymorph phases, Appl. Surf. Sci. 496 (2019) 143671. https://doi.org/10.1016/j.apsusc.2019.143671.

[41] A.O.S. Silva, M.J.B. Souza, A.S. Araujo, Hydrothermal synthesis and thermal characterization of niobium-aluminophosphate with AEL structure, Int. J. Inorg.

Mater. 3 (2001) 461–466. https://doi.org/10.1016/S1466-6049(01)00043-5.

[42] M.J.B. Souza, A.O.S. Silva, F.J. Fernandes, A.S. Araujo, Acid properties of AIMCM-41 molecular sieves with different silica-alumina ratios by thermogravimetry, J. Therm. Anal. Calorim. 79 (2005) 425–428. https://doi.org/10.1007/s10973-005-0078-y.

[43] A.S. Araujo, V.J. Fernandes, I. Giolito, L.B. Zinner, Evaluation of the relative acid strength of cerium and calcium exchanged Y zeolite by TG and DSC, Thermochim. Acta. 223 (1993) 129–134. https://doi.org/10.1016/0040-6031(93)80127-V.

[44] G.J.T.F. V. J. Fernandes, A. S. Araujo, Thermal Analysis Applied to Solid Catalysts Acidity, Activity and Regeneration, J. Therm. Anal. Calorim. 56 (1999) 275–285. https://doi.org/10.1023/A:1010121928160.

[45] S. Meiboom, D. Gill, Modified spin-echo method for measuring nuclear relaxation times, Rev. Sci. Instrum. 29 (1958) 688–691. https://doi.org/10.1063/1.1716296.

[46] R.W. Schurko, Ultra-wideline solid-state NMR spectroscopy, Acc. Chem. Res. 46 (2013) 1985–1995. https://doi.org/10.1021/ar400045t.

[47] L.A. O'Dell, The WURST kind of pulses in solid-state NMR, Solid State Nucl. Magn. Reson. 55–56 (2013) 28–41. https://doi.org/10.1016/j.ssnmr.2013.10.003.

[48] M. Thommes, K. Kaneko, A. V Neimark, J.P. Olivier, F. Rodriguez-Reinoso, J. Rouquerol, K.S.W. Sing, Physisorption of gases, with special reference to the evaluation of surface area and pore size distribution (IUPAC Technical Report), Pure Appl. Chem. 87 (2015) 1051–1069. https://doi.org/doi:10.1515/pac-2014-1117.

[49] M. Kruk, M. Jaroniec, C.H. Ko, R. Ryoo, Characterization of the porous structure of SBA-15, Chem. Mater. 12 (2000) 1961–1968. https://doi.org/10.1021/cm000164e.

[50] A.A.S. Gonçalves, Development of Nanostructured Ceramic Catalysts Based on Mixed Metal Oxides, Doctoral Dissertation, Kent State University, 2018. http://rave.ohiolink.edu/etdc/view?acc_num=kent1543412496976455.

[51] M. Jaroniec, M. Kruk, J.P. Olivier, Standard nitrogen adsorption data for characterization of nanoporous silicas, Langmuir. 15 (1999) 5410–5413. https://doi.org/10.1021/la990136e.

[52] M. Kruk, M. Jaroniec, R.K. Gilpin, Y.W. Zhou, Nitrogen adsorption studies of coated and chemically modified chromatographic silica gels, Langmuir. 13 (1997) 545–550. https://doi.org/10.1021/la960881g.

[53] A.C.F. Coriolano, C.G.C. Silva, M.J.F. Costa, S.B.C. Pergher, V.P.S. Caldeira, A.S. Araujo, Development of HZSM-5/AlMCM-41 hybrid micro-mesoporous material and application for pyrolysis of vacuum gasoil, Microporous Mesoporous Mater. 172 (2013) 206. https://doi.org/10.1016/j.micromeso.2013.01.022.

[54] M.J.F. Costa, J. Marszewska, A.A.S. Gonçalves, L.K.C. De Souza, A.S. Araujo, M. Jaroniec, Microwave-assisted single-surfactant templating synthesis of mesoporous zeolites, RSC Adv. 6 (2016). https://doi.org/10.1039/c6ra06554f.

[55] K.O. Drake, D. Carta, L.J. Skipper, F.E. Sowrey, R.J. Newport, M.E. Smith, A multinuclear solid state NMR study of the sol-gel formation of amorphous Nb_2O_5-SiO_2 materials, Solid State Nucl. Magn. Reson. 27 (2005) 28–36. https://doi.org/10.1016/j.ssnmr.2004.08.008.

[56] A.L. Wübker, J. Koppe, H. Bradtmüller, L. Keweloh, D. Pleschka, W. Uhl, M.R. Hansen, H. Eckert, Solid-State Nuclear Magnetic Resonance Techniques for the Structural Characterization of Geminal Alane-Phosphane Frustrated Lewis Pairs and Secondary Adducts, Chem. - A Eur. J. 27 (2021) 13249–13257. https://doi.org/10.1002/chem.202102113.

[57] J.B. d'Espinose de Lacaillerie, C. Fretigny, D. Massiot, MAS NMR spectra of quadrupolar nuclei in disordered solids: The Czjzek model, J. Magn. Reson. 192 (2008) 244–251. https://doi.org/10.1016/j.jmr.2008.03.001.

[58] O.B. Lapina, D.F. Khabibulin, A.A. Shubin, V. V. Terskikh, Practical aspects of 51V and 93Nb solid-state NMR spectroscopy and applications to oxide materials, Prog. Nucl. Magn. Reson. Spectrosc. 53 (2008) 128–191. https://doi.org/10.1016/j.pnmrs.2007.12.001.

[59] E. Papulovskiy, D.F. Khabibulin, V. V. Terskikh, E.A. Paukshtis, V.M. Bondareva, A.A. Shubin, A.S. Andreev, O. Lapina, Effect of impregnation on the structure of niobium oxide/alumina catalysts studied by multinuclear solid-state NMR, FTIR, and quantum chemical calculations, J. Phys. Chem. C. 119 (2015) 10400–10411. https://doi.org/10.1021/acs.jpcc.5b01616.

[60] E. Papulovskiy, A.A. Shubin, V. V. Terskikh, C.J. Pickard, O.B. Lapina, Theoretical and experimental insights into applicability of solid-state 93Nb NMR in catalysis, Phys. Chem. Chem. Phys. 15 (2013) 5115–5131. https://doi.org/10.1039/c3cp44016h.

[61] A. Flambard, L. Montagne, L. Delevoye, S. Steuernagel, 93Nb and 17O NMR chemical shifts of niobiophosphate compounds, Solid State Nucl. Magn. Reson. 32 (2007) 34–43. https://doi.org/10.1016/j.ssnmr.2007.07.001.

[62] O.B. Lapina, D.F. Khabibulin, K. V. Romanenko, Z. Gan, M.G. Zuev, V.N.

Krasil'nikov, V.E. Fedorov, 93Nb NMR chemical shift scale for niobia systems, Solid State Nucl. Magn. Reson. 28 (2005) 204–224. https://doi.org/10.1016/j.ssnmr.2005.09.003.

[63] J.N. Chheda, Y. Román-Leshkov, J.A. Dumesic, Production of 5-hydroxymethylfurfural and furfural by dehydration of biomass-derived mono- and poly-saccharides, Green Chem. 9 (2007) 342–35. https://doi.org/10.1039/b611568c.

[64] E.I. Gürbüz, S.G. Wettstein, J.A. Dumesic, Conversion of hemicellulose to furfural and levulinic acid using biphasic reactors with alkylphenol solvents, ChemSusChem. 5 (2012) 383–387. https://doi.org/10.1002/cssc.201100608.

[65] R. Carrasquillo-Flores, M. Käldström, F. Schüth, J.A. Dumesic, R. Rinaldi, Mechanocatalytic depolymerization of dry (Ligno)cellulose as an entry process for high-yield production of furfurals, ACS Catal. 3 (2013) 993–997. https://doi.org/10.1021/cs4001333.

[66] K. Nakajima, Y. Baba, R. Noma, M. Kitano, J. N. Kondo, S. Hayashi, M. Hara, $Nb_2O_5 \cdot nH_2O$ as a heterogeneous catalyst with water-tolerant lewis acid sites, J. Am. Chem. Soc. 133 (2011) 4224–4227. https://doi.org/10.1021/ja110482r.

[67] I. Delidovich, R. Palkovits, Catalytic Isomerization of Biomass-Derived Aldoses: A Review, ChemSusChem. 9 (2016) 547–561. https://doi.org/10.1002/cssc.201501577.

Declaration of interests

☒The authors declare that they have no known competing financial interests or personal relationships that could have appeared to influence the work reported in this paper.

☐The authors declare the following financial interests/personal relationships which may be considered as potential competing interests: